Scaling study of the combustion performance of gas–gas rocket injectors*

Wang Xiao-Wei(汪小卫), Cai Guo-Biao(蔡国飙)†, and Jin Ping(金 平)

School of Astronautics, Beijing University of Aeronautics and Astronautics, Beijing 100191, *China*

(Received 16 March 2011; revised manuscript received 16 May 2011)

To obtain the key subelements that may influence the scaling of gas–gas injector combustor performance, the combustion performance subelements in a liquid propellant rocket engine combustor are initially analysed based on the results of a previous study on the scaling of a gas–gas combustion flowfield. Analysis indicates that inner wall friction loss and heat-flux loss are two key issues in gaining the scaling criterion of the combustion performance. The similarity conditions of the inner wall friction loss and heat-flux loss in a gas–gas combustion chamber are obtained by theoretical analyses. Then the theoretical scaling criterion was obtained for the combustion performance, but it proved to be impractical. The criterion conditions, the wall friction and the heat flux are further analysed in detail to obtain the specific engineering scaling criterion of the combustion performance. The results indicate that when the inner flowfields in the combustors are similar, the combustor wall shear stress will have similar distributions qualitatively and will be directly proportional to $p_c^{0.8} d_t^{-0.2}$ quantitatively. In addition, the combustion peformance will remain unchanged. Furthermore, multi-element injector chambers with different geometric sizes and at different pressures are numerically simulated and the wall shear stress and combustion efficiencies are solved and compared with each other. A multi-element injector chamber is designed and hot-fire tested at several chamber pressures and the combustion performances are measured in a total of nine hot-fire tests. The numerical and experimental results verified the similarities among combustor wall shear stress and combustion performances at different chamber pressures and geometries, with the criterion applied.

Keywords: scaling, combustion performance, subscale combustor wall friction, gas–gas combustion

PACS: 47.70.–n, 84.60.Bk, 62.40.+i, 28.50.Ky **DOI:** 10.1088/1674-1056/20/10/104701

1. Introduction

The scaling technique of liquid propellant rocket engine (LPRE) combustion devices generally contains scaling of the inner combustion flow, heat transfer and combustion performance,[1−3] among them combustion performance is a combination of engineering parameters influenced by many factors, which cannot be investigated directly. Thus, scaling of combustion performance is always the most difficult to study. The scaling technique of LPRE combustion performance was generally investigated and reviewed in Refs. [1]–[3], while no scaling criterion had been obtained.

A full flow stage combustion (FFSC) cycle engine is preferable because of its high performance and high reliability.[4] Gas–gas combustion technology is a key technology for this kind of engine. The FFSC nominal gas–gas injector main thrust chamber was designed at a chamber pressure of above 20 MPa and a mass flowrate of above 450 kg/s. Also, gas–gas injectors have been widely used on other engines and combustion devices.[5,6] Thus it will be of great value if a feasible scaling technique can be applied to the development of gas–gas injector combustors. And although a lot of studies have been carried out on gas–gas injectors with a background of FFSC,[6−28] the scaling of a gas–gas combustor, unfortunately, has only just begun. Cai and Wang *et al.*[25−27] studied the scaling of the inner combustion flowfield in a gas–gas injector combustor and the corresponding scaling criterion was obtained. The criterion indicates that the combustion flowfields can be similar when the geometries are similar and the chamber pressure is variable. However, in the engineering development applications of LPREs, good heat transfer and combustion performance are always the objectives of engineering designers.[1−6,11−14] Based on a study on scaling of the inner combustion flowfield, Wang *et al.*[28] succes-

Project supported by the National High Technology Research and Development Program of China (Grant No. 2009AA702) and the Innovation Foundation of Beijing University of Aeronautics and Astronautics for PhD Graduates (Grant No. 430569).

†Author to whom any correspondence should be addressed. E-mail: cgb@buaa.edu.cn

© 2011 Chinese Physical Society and IOP Publishing Ltd

sively studied the scaling of heat transfer in gas–gas injector combustor. Unlike inner flowfield, the combustion performance is a complicated combination parameter and lots of factors in the combustor, including heat transfer, influence combustion performance, thus combustion performance is always the hardest parameter to analyse and obtain just by measurement in the tests. However, gas–gas combustion is a straightforward mixing and reaction process and the characteristics of the gas–gas injector chamber and the existence of similarity of flowfield show that is is possible to analyse the scaling of combustion performance. This paper focuses on the scaling technology of the combustion performance of a gas–gas injector combustor. The scaling criterion, i.e., how to use low-pressure small-sized model engine combustion performance data to predict the combustion performance of high-pressure large-size prototype engines, will be determined.

As a combination engineering parameter, the combustion performance cannot be investigated directly. In this study, the combustion performance subelements will be analysed initially to discover the factors that play key roles in the combustion performance and locate the specific research objects. Theoretical, numerical and experimental studies will be conducted to obtain and validate the scaling criterion of the combustion performance.

2. Performance subelement analysis

The various subelements that comprise LPRE combustor performance have been previously defined in a number of widely available papers.[3,29−31] Combustion performance losses in an LPRE gas–gas injector combustor can be broken down into several basic categories:[3]

1) the collective inefficiencies of the core and barrier injection elements;

2) the surface boundary losses:

(a) heat energy losses from the fluids to the chamber walls,

(b) boundary layer losses (effect of wall boundaries on the flow streams);

3) unintentional maldistribution losses;

4) intentional maldistribution losses.

All combustors include some forms of almost all of the first and third categories of losses. The results in Refs. [25]–[27] indicate that the combustion flowfield can be kept similar when some conditions are satisfied. Based on the similarity of the gas–gas combustion flowfield, the performance subelements given above are analysed as follows.

All parts of the first category belong to the mixing and combustion of inner combustion flowfield, thus they will be the same when the inner flowfields are similar.

The third category is the unintentional maldistribution losses caused by some random errors or other factors, which are always unavoidable in any engine. However, this kind of loss is always very small and the error will have limited influence on the flowfield. In addition, because the flows in the injectors are always in a turbulent state, the study in Refs. [25]–[27] indicated that the maldistributions at the injector inlets or from the injector manifolding will not influence the parameter distributions at the injector outlets, thus they will not influence the inner combustion flowfield. Overall this category of loss can be considered as a minor factor even though there are some influences. This study does not consider this kind of loss. In addition, even though unintentional maldistribution losses play a very important role in combustion performance, they are not within the scope of this study.

The fourth category is the intentional maldistribution losses, which belong to the inlet conditions of the combustion flowfield in the combustor. Since they are intentional, it is easy to keep these inlet conditions similar, which is also a precondition of the similarity of the inner flowfield, thus the losses can be kept the same.

As for the second category of losses, the similarity of the inner main flowfield cannot ensure the similarity of heat energy loss and the wall boundary layer loss. Here, the wall boundary layer loss is just the wall-friction loss in an LPRE combustor. How these two factors contribute to gas–gas injector combustor performance is not yet clear. Therefore, these two kinds of losses will be studied in detail in the following parts.

References [25]–[27] mainly focused on the similarity of main flow, ignoring the thin boundary layer. However, on the basis of similarity of the main flow, the scaling of wall boundary friction and heat transfer totally depends on the similarity of the boundary layer flow. Thus, the formulation analysis of the boundary layer equations and dimensional analysis of the inner wall boundary friction and heat-transfer phenomena

in a gas–gas combustion chamber will be carried out in this paper to reveal the similarity condition of inner wall friction and heat transfer.

The formulation analysis of the boundary layer equations has been carried out in Ref. [28]. And the result indicates that the key to ensure the similarities of the boundary layer equations and the monodromy conditions is to keep Re (defined below) unchanged, because there is no self-similar characteristic for the boundary layer flow. Re must be kept constant for similarity of boundary layer flows.

3. Dimensional analysis

Dimensional analysis is another important theoretical method which can effectively serve the experimental studies. This method has a wide applicability;[27−34] unfortunately, its application to the phenomena in LPREs is less well documented these days. Without considering the reaction in the boundary layer, the parameters related to the wall boundary layer flow phenomenon in an LPRE include: velocity u, temperature T, diameter D, pressure p, and fluid property parameters (density ρ, viscosity μ, specific heat C_p and thermal conductivity λ).

The specific monodromy conditions determine the unique solutions of the same kind of physical phenomena. When the main flowfield is identified, the pressure p in the boundary layer is also identified as the same as the main flow.[33] And the high temperature gas in the combustor can be treated as an ideal gas, thus the density and temperature become dependent on each other. Therefore, the independent parameters related to the inner wall friction and heat-transfer phenomena in an LPRE can be obtained: the main flow velocity u, diameter D and the property parameters (ρ, μ, λ, C_p).

The dimensional analysis of the heat-transfer phenomenon has also been carried out in Ref. [28] and the result indicates that Nu number will be the same as long as Re is constant. Here, the wall friction will be further analysed using dimensional analysis. The wall-friction stress $\tau_{\rm w}$ is chosen as the research object for the wall-friction phenomenon and an expression for $\tau_{\rm w}$ will be obtained with the π theorem.

The basic units for these parameters are L (length), T (time), and M (mass), and u, D, and ρ are chosen as the basic parameters. As a result, for the application of the π theorem, two dimensionless parameters are introduced as follows:

$$\pi_1 = \frac{\tau_{\rm w}}{\rho u^2}, \quad \pi_2 = \frac{\rho u D}{\mu} = Re.$$

In fact, here $\tau_{\rm w}/\rho u^2 = V_*^2/u^2 = \lambda/8$, where V_* is the friction velocity and λ is the friction factor, and they are related as $\lambda = 8V_*^2/u^2$.[33] Thus, the following expression can be obtained

$$\lambda = f(Re). \tag{1}$$

Equation (1) indicates that the wall-friction loss will be the same as long as Re is kept constant. This result is the same as that of the formulation analysis.

Theoretical analysis shows that Re needs to remain unchanged to ensure the similarity of the wall friction and heat transfer in a gas–gas injector combustor. This result can lead to a perfect scaling technology of the combustion performance.

In Ref. [28], the theoretical scaling criterion of keeping Re constant in an LPRE combustor has been analysed and the result shows that Re is directly proportional to pD, which implies that to keep Re constant the pressure must be inversely proportional to the size. This scaling method becomes impractical if low pressure hot tests are employed to simulate the high-pressure ones, since impractical larger-size combustion chambers would be needed, which cannot exhibit the value of the scaling technology. Therefore, the perfect scaling relationship cannot always be easily achieved because it is hard to keep Re unchanged in practical engineering applications.

Because local normal boundary layer flow structures become dissimilar when Re changes, different λ are produced and the quantitative theoretical scaling method of wall-friction stress does not exist with different Re. However, similarity of the main combustion flowfield can be obtained in LPRE combustors with different Re,[25−27] and the wall boundary conditions are always satisfied, which means that both the inner (i.e. the wall) and outer (i.e. the main flow) boundary conditions of boundary layer flowfield can be satisfied regardless of Re. Thus, though different Re can produce local quantitatively dissimilar wall-friction stress, the qualitatively similar wall-friction stress distribution along the combustor wall always exists when the main flowfield is similar. But as a key subelement of the combustion performance, qualitative similarity is not enough, the quantitative practicable scaling method still needs to be solved.

The above analyses indicate that it is impractical to carry out the scaling of gas–gas combustion performance through ensuring constant Re, though a qualitative similarity can be obtained for λ and Nu.[28] Since a theoretical scaling technology, like that of the main flowfield obtained in Refs. [25]–[27], cannot be obtained, detailed specific analyses about the effects of the wall friction and heat transfer on the combustion performance in LPRE will be conducted. Whether there are some other engineering methods that can also obtain the quantitatively scaling criterion to avoid the theoretical requirement for Re will also be explained.

4. Specific criterion analysis

All the following analyses are based on whether the scaling conditions of the gas–gas combustion flowfield are satisfied when the chamber pressure and size are changed.

4.1. The wall friction

The most popular method for calculating the turbulent boundary layer friction is Prandtl's method, which has been validated when Re is less than 3.4×10^6,[33]

$$\frac{1}{\sqrt{\lambda}} = 0.87\ln(Re\sqrt{\lambda}) - 0.8, \tag{2}$$

where $\lambda \propto Re^{-0.2}$ was obtained after curve-fitting this equation ($4000 < Re < 3.4\times10^6$), then the following result can be obtained

$$\tau_{\rm w} = \frac{1}{8}\lambda\rho U_0^2 \propto Re^{-0.2}\rho U_0^2 \propto p^{0.8}d_{\rm t}^{-0.2}. \tag{3}$$

The friction loss $\zeta_{\rm f}$ on combustion performance can be expressed as follows:

$$\zeta_{\rm f} = \frac{F_{\rm w}}{F} \propto p_{\rm c}^{-0.2}d_{\rm t}^{-0.2}. \tag{4}$$

Here, $F_{\rm w}$ is the friction force with $F_{\rm w} \propto \tau_{\rm w}A \propto p_{\rm c}^{0.8}d_{\rm t}^{1.8}$ and F is the thrust of the combustion chamber with $F \propto p_{\rm c}d_{\rm t}^2$. From Eq. (4), it can be seen that when the main flowfield is similar, the friction loss becomes directly proportional to $p_{\rm c}^{-0.2}d_{\rm t}^{-0.2}$.

4.1.1. Similar physical geometry

When a small-sized low-pressure model engine is used to scale a full-scale high-pressure engine, the easiest way is to keep the physical geometry profile of the small combustion chamber similar to the full-scale one. The main flow of these two chambers can be kept similar when the scaling conditions of the main flow is satisfied,[25–27] while the wall-friction loss $\zeta_{\rm f}$ is directly proportional to $p_{\rm c}^{-0.2}d_{\rm t}^{-0.2}$. Thus, if the friction loss of the model engine is obtained, that of the full-scale engine can be obtained directly using Eq. (4). However, the friction loss is always hard to be identified or measured. On the other hand, Eq. (4) also indicates that the effects of the pressure and size on friction loss are slight. Even when an extreme scaling condition is applied, i.e., the pressure of the model engine is one-tenth that of the prototype one and it is half the size, then $\zeta_{\rm f}$ of the prototype engine is 0.55 times lower than that of the model engine. In addition, the wall-friction loss itself in an LPRE chamber is always very small, generally it ranges from 0.005 to 0.02,[35] then $\zeta_{\rm f}$ of the prototype engine is just $0.55\times(0.005\sim0.02) = 0.00275\sim0.011$. The change between these two friction losses is just $0.00225\sim0.009$, which can be ignored in hot-tests. Therefore, in general, the change of the friction loss caused by the change of the chamber pressure and size can be ignored, even though a similar physical geometry profile is used.

4.1.2. Dissimilar physical geometry

It is convenient to use the similar geometry profile in the scaling method. While, if an improved requirement for performance loss is demanded or the friction loss has to be calculated from model engine to prototype, the similar physical profile cannot be used due to the difficulty of measurement of friction loss in the tests. Thus, a calculation of this kind of loss from model to prototype becomes a problem. Since it becomes impossible to accurately define the friction loss coming from the wall boundary layer flow, we have to examine whether or not another scaling method can be found that avoids the effect of the wall boundary layer friction loss on the combustion performance.

In the design of combustion chamber for an LPRE, especially for the nozzle, the non-viscous flow profile is figured out directly according to the requirement of the main flow, then the physical nozzle profile is obtained from a correction of this non-viscous flow profile by considering the effect of the wall boundary layer flow,[35] as shown in Fig. 1. The dashed line is the non-viscous flow profile and the solid line is the physical profile. The coordinates of the physical pro-

file are as follows:

$$r = r_{\rm pot} + \delta^* \cos\alpha,$$
$$x = x_{\rm t} - \delta^* \sin\alpha. \quad (5)$$

Here, δ^* is the boundary layer displacement thickness, $r_{\rm pot}$ and $x_{\rm pot}$ are coordinates of the non-viscous flow profile. This design of the combustor physical profile ensures the maximum flowrate through the nozzle and totally avoids the effect of wall boundary layer friction on the combustion performance. In this method, the non-viscous flow profiles need be kept similar, then the correction wall profile will be calculated separately according to the specific *Re* of the model and prototype engines. Because the *Re* values of model and prototype engines are different, the physical wall profiles for the model and prototype will be a little different.

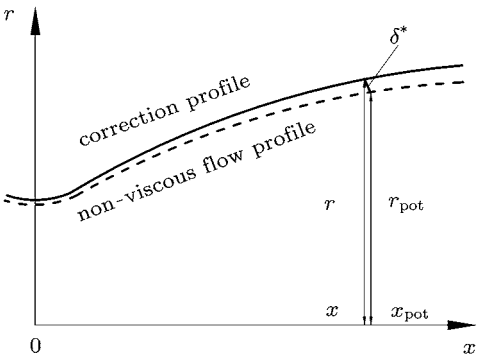


Fig. 1. Correction of the nozzle profile in consideration of the effect of the wall boundary layer.

Therefore, if this correction design is used in the scaling of combustion performance, though the design of the model combustor becomes more complicated, the effect of wall-friction loss on combustion performance will not be considered at all.

4.2. The heat flux

4.2.1. Regenerative cooling chamber

Though the heat transfer from the combustion flow to inner wall always exists, when regenerative cooling chambers are used in both model and prototype engines, in the end the heat will go back to the combustor completely. Thus, the heat-transfer loss also does not exist any more in this condition.

4.2.2. Non-regenerative cooling chamber

If the prototype does not use the regenerative cooling method, the heat transfer directly through the inner wall becomes the combustion performance loss. The study on the scaling of heat transfer in Ref. [28] indicates that the inner wall heat flux correlates well with pressure and dimension as $q \propto p_{\rm c}^{0.8} d_{\rm t}^{-0.2}$ when the inner combustion flowfield is similar. Thus, the heat transfer loss ζ_q can be obtained

$$\zeta_q \propto \sqrt{\left(\frac{Q}{\dot{m}}\right)} \propto \sqrt{\frac{Q}{p_{\rm c} d_{\rm t}^2}}$$
$$\propto \sqrt{p_{\rm c}^{-0.2} d_{\rm t}^{-0.2}} \propto p_{\rm c}^{-0.1} d_{\rm t}^{-0.1}, \quad (6)$$
$$Q \propto q d_{\rm t}^2 \propto p_{\rm c}^{*0.8} d_{\rm t}^{1.8}. \quad (7)$$

Here, Q is the heat-transfer quantity from the inner wall, $\dot{m}$ is the total propellant flowrate. Because ζ_q is directly proportional to $p_{\rm c}^{-0.1} d_{\rm t}^{-0.1}$, the changes of chamber pressure and size will have little influence on the heat transfer loss. Even though the pressure of the model is one-tenth that of prototype engine and it is half the size, the ζ_q of prototype engine is 0.74 times that of the model engine. In addition, like the wall-friction loss analysed in subsubsection 4.1.1, the heat-transfer loss is always small except in a micro or very small-sized combustor, thus the change of ζ_q in the model and prototype engines is also very small and can also be ignored.

In conclusion, from all the above analyses, generally, when the scaling criterion of the inner gas–gas combustion flowfield is satisfied, the combustion performance will also remain unchanged. The scaling criterion of the gas–gas combustion flowfield is as follows: (a) similarity between the geometries of the injector and the chamber; (b) identical propellants; (c) constant injection velocities and propellant temperatures; (d) non-slip and similar species wall boundary; (e) flow in laminar or sufficient turbulence conditions.

5. Numerical study

Model and prototype multi-element gas–gas injector chambers were designed and gaseous oxygen and gaseous hydrogen were chosen as the propellants. The shear-coaxial injector, which has been widely applied in H_2/O_2 LPREs, was used. First, chamber pressure was kept constant and the prototype and model chambers had different sizes. Second, the sizes were kept constant and the chambers were designed at different pressures. The chamber parameters were chosen from the operating range of real engines. The characteristic length of the chamber was 935 mm and the contract ratio was 3.7. The prototype injector element structure and the chamber are shown in Fig. 2.

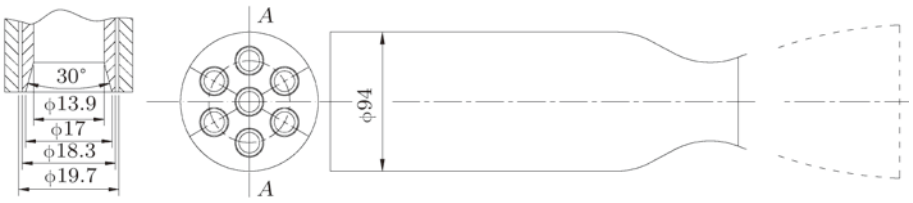


Fig. 2. Prototype shear-coaxial injector element and chamber.

5.1. Numerical method and boundary condition

The numerical modeling method has been analysed in Refs. [27] and [28], and the same method is used here. The steady Reynolds Average Navier–Stokes (RANS) method combined with a k–ε turbulence model was used to study different conditions in statistical states. The entire system was solved by a strongly coupled implicit time-marching method, using ADI factorization for the inversion of the implicit operator. Convective terms were 2-order flux split upwind differenced, whereas diffusion terms were centrally differenced.

As a result of the non-axisymmetric nature of the injector element, a 60° pie section of the chamber, encompassing a complete element, was modelled. The radial and the axial stretchings of the grid were used near the wall boundary and in the shear layer domain. The inlets had a fixed mass flowrate and the inlet turbulence intensities were both set to 5%. The nozzle exit was specified as a supersonic outlet. Adiabatic non-slip wall boundaries were used on the chamber walls. Two symmetric sides of the model were set as symmetric boundaries.

5.2. Geometric scaling analysis

In the calculation of geometric scaling, the nominal chamber pressures were kept at 3.0 MPa. The model was designed by reducing all the lengths of the prototype by a universal linear scale factor of 2.0. The parameters are shown in Table 1, indicating that the scaling criterion of the inner combustion flowfield is satisfied. Then solutions were obtained to achieve steady state convergences. The results are shown in Figs. 3–5 and Table 2.

Table 1. Parameters of model and prototype chambers.

Type	Scale factor L	H_2 flowrate /g·s^{-1}	H_2 temperature/K	H_2 injection velocity/m·s^{-1}	O_2 flowrate /g·s^{-1}	O_2 temperature/K	O_2 injection velocity/m·s^{-1}
Prototype	2	421.4	300	∼ 550	2528.4	300	∼ 60
Model	1	105.35	300	∼ 550	632.1	300	∼ 60

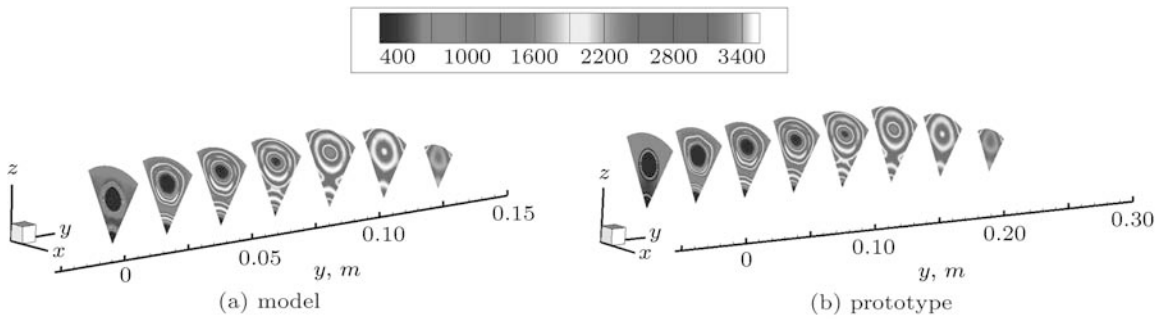


Fig. 3. Temperature contours for some axial sections in the two chambers (K).

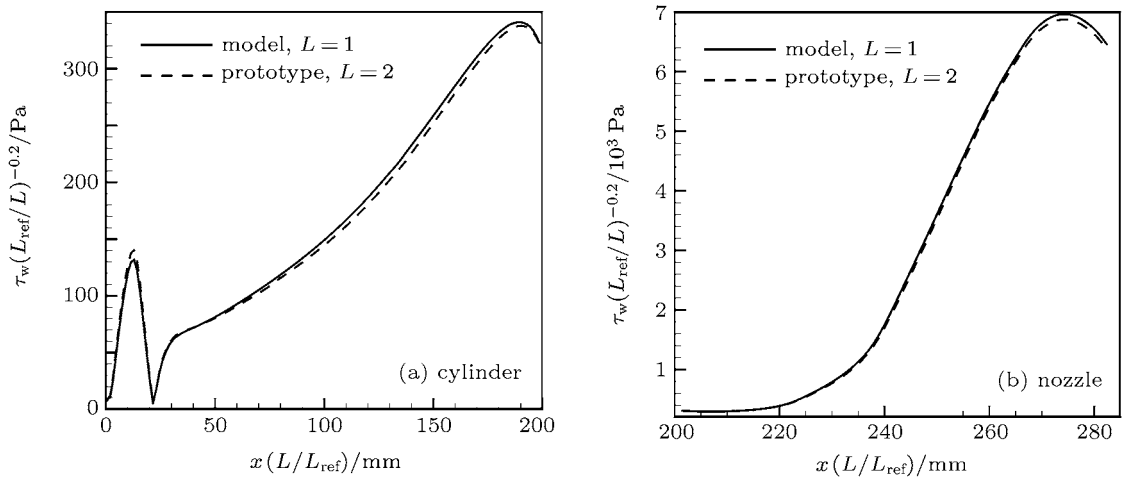


Fig. 4. The wall shear stress (scaled with respect to $(1/L)^{-0.2}$) versus axial distance at the A–A section for the two chambers.

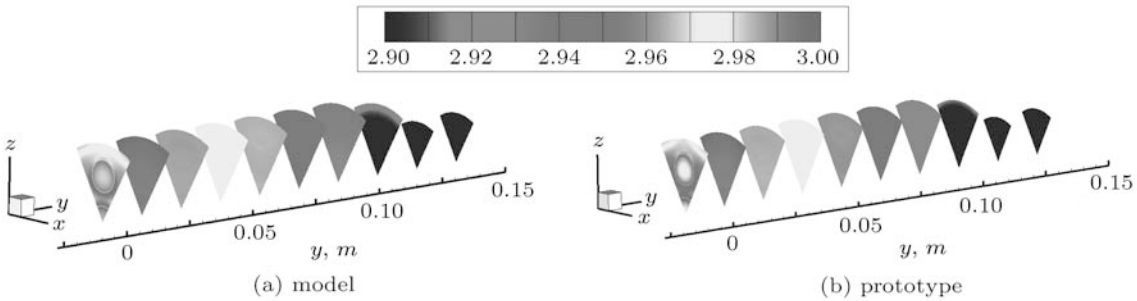


Fig. 5. Pressure contours on some axial sections in the two chambers (MPa).

Table 2. Numerical results of model and prototype chambers.

Type	p_c/Pa	Wall friction force F_w/N	C^*/m·s^{-1}	Thrust F/N
Prototype	2973667	45.1	2224	8296
Model	2959816	13.2	2214	2082

The temperature contours of the two chambers in Fig. 3 indicate an apparent similarity of the flowfield. Figures 4 and 5 show the wall shear stress distributions and the chamber pressure contours respectively. In Fig. 4, according to Eq. (3), the wall shear stress is scaled with respect to $(L_{ref}/L)^{-0.2}$ to compare quantitatively, here L_{ref} is chosen as 1.0. The distributions are set at the axial location on the A–A section as shown in Fig. 2 to represent the characteristics of the whole distribution on the combustors. The x-coordinates have also been scaled with respect to (L/L_{ref}) to compare them more conveniently. It can be seen that the wall shear stress has the same distribution for the two chambers and after the scaling operations their values are almost the same at any location of the combustor, which verifies the theoretical results in subsection 4.1: $\tau_w \propto p^{0.8} d_t^{-0.2}$. When the wall shear stress is an important investigative objective, this result is of great value. But in the engineering design and development of an LPRE engine, the wall-friction force has a minor influence on the combustor thrust, which can be seen in Table 2. The wall friction force can be ignored when compared to the whole thrust of the combustor, which also verifies the analysis result in subsection 4.1.

Furthermore, in an LPRE engine, the combustion performance is always represented with C^* efficiency, which can be calculated with the chamber pressure in the following equation

$$C^* = \frac{p_c A_t}{\dot{m}}. \tag{8}$$

Here, p_c is the chamber pressure, A_t is the area of

the nozzle throat and $\dot{m}$ is the total propellant mass flowrate. In this numerical study, $A_t/\dot{m}$ is the same for these two chambers, thus the C^* efficiency merely depends on the chamber pressure. Figure 5 shows the chamber pressure distributions at some axial locations in chambers. The pressure distributions are almost the same in the two cases, which indicates the combustion performances are the same. Table 2 lists the chamber pressure p_c, C^* and the thrust of the two chambers. p_c is the area-weighted average pressure of the combustor cross-section at the end of the cylinder and C^* is calculated from p_c. The thrust is calculated based on the following equation

$$F = \int p \, \mathrm{d}A \propto p_c d_t^2. \tag{9}$$

Here, p is the pressure of the inner flow on the inner wall.

It can be seen that C^* of these two chambers are almost the same. When the pressure distributions are the same, the thrust will be proportional to d_t^2 according to Eq. (9). Thus, the thrust of the prototype chamber can be calculated from that of the model as $2082\ \mathrm{N} \times 4.0 = 8328\ \mathrm{N}$, which is very close to the real one (8296 N) listed in Table 2.

5.3. Pressure scaling analysis

In the calculation of pressure scaling, the dimensions of the chambers were kept unchanged. The prototype chamber studied above was chosen and the calculation conditions are shown in Table 3, in which three extreme pressures are selected to investigate the greatest distinction and the changing tendency of results. The parameters in Table 3 indicate that the scaling criterion of the combustion flowfield was satisfied. The results are shown in Figs. 6–8 and Table 4.

Table 3. Parameters of pressure scaling conditions.

Chamber pressure/MPa	H_2 flowrate/g·s^{-1}	H_2 temperature/K	H_2 injection velocity/m·s^{-1}	O_2 flowrate/g·s^{-1}	O_2 temperature/K	O_2 injection velocity/m·s^{-1}
1	0.1405	300	~ 550	0.8428	300	~ 60
10	1.4047	300	~ 550	8.428	300	~ 60
20	2.8094	300	~ 550	16.856	300	~ 60

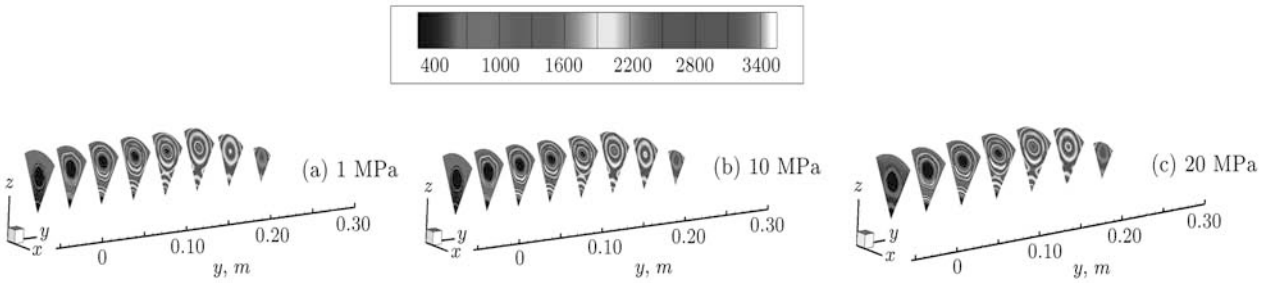


Fig. 6. Temperature contours on some axial sections of the three chambers (K).

The temperature contours of the two chambers in Fig. 6 indicate an apparent similarity among these cases. Figures 7 and 8 show respectively the wall shear stress distributions and the chamber pressure contours. In Fig. 7, according to Eq. (3), the wall shear stress is scaled with respect to $(p_{\mathrm{ref}}/p_c)^{-0.8}$ to compare quantitatively, here p_{ref} is chosen as 1.0 MPa. The distributions are at the axial location on the A–A section as shown in Fig. 2 to represent the characteristics of the whole distribution on the combustors. The x-coordinates are not scaled because they are the same for the three chambers. It can be seen that the wall shear stress has the same distribution for these chambers and after the scaling operations their values are almost the same at any location of the combustor, which verifies the theoretical results in subsection 4.1: $\tau_w \propto p^{0.8} d_t^{-0.2}$. Like the analysis in subsection 5.2, in an LPRE engine, the wall-friction force can be ignored when compared to the combustor thrust, which can be seen in Table 4.

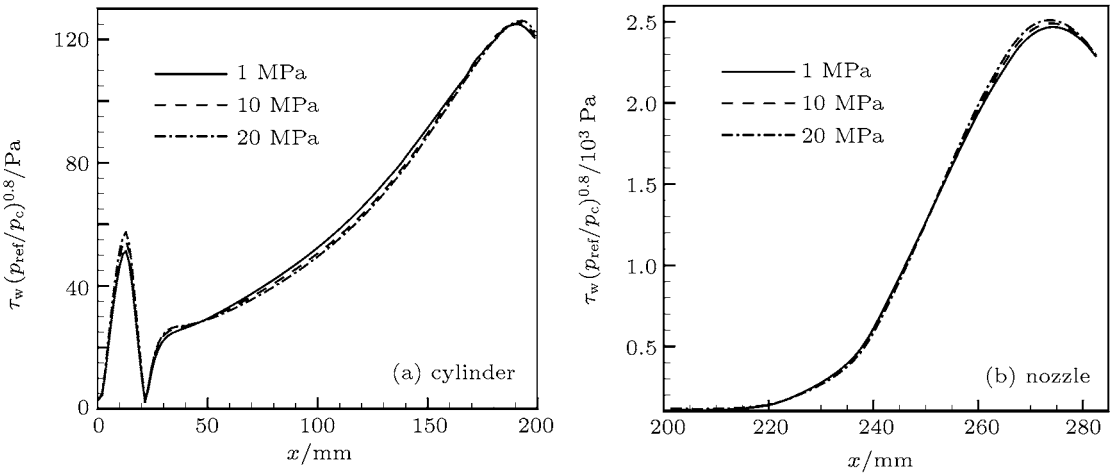


Fig. 7. The wall shear stress (scaled with respect to $(1.0\ \text{MPa}/p_c)^{0.8}$) versus axial distance at the A–A section for the three chambers.

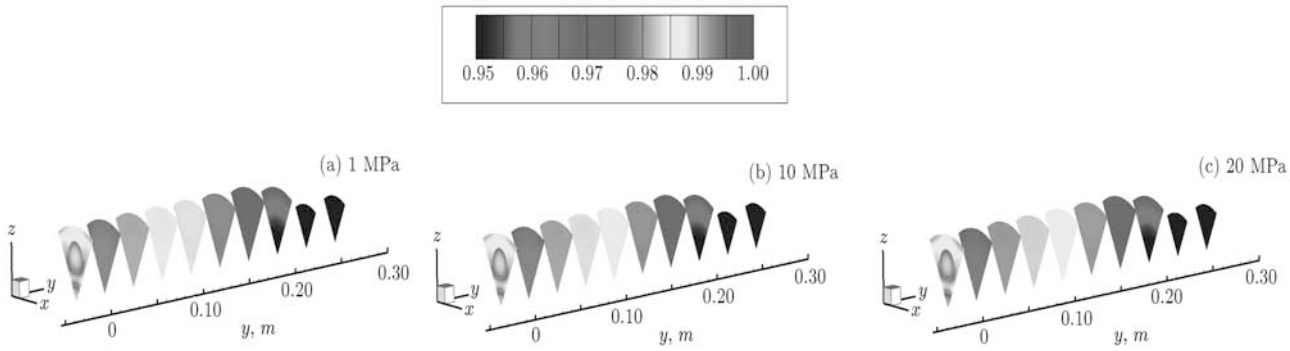


Fig. 8. Ratios of pressure results to the nominal chamber pressures on some axial sections of the three chambers.

Table 4. Numerical results of the three chambers.

Case no.	nominal chamber pressure/MPa	p_c/MPa	Wall shear force F_w/N	C^*/m·s^{-1}	Thrust/N
1	1	1003954	18.8	2252	2782
2	10	10041347	118.8	2253	28084
3	20	20105180	207.6	2255	56212

Figure 8 shows the chamber pressure distributions at some axial locations in chambers. The pressure distributions are almost the same at the three pressures, which indicates the combustion performances are the same. To compare the results of these cases quantitatively, like in Table 2, Table 4 further lists p_c and C^*, and the thrust in these cases. The results show that C^* of these chambers are almost the same. According to Eq. (9), when the chamber sizes are the same, the thrust will be proportional to p_c. Thus, the thrusts in cases 2 and 3 can be calculated from that of case 1 to be 2782 N $\times$ 10 (and 20) = 27820 (or 55640) N, which are very close to the real ones listed in Table 4.

6. Experimental study

Up to now, no experimental study focused on the scaling of gas–gas combustion chamber performance has been found. In this study a multi-element shear coaxial injector and a combustion chamber were designed, fabricated, and hot-fire tested at different chamber pressures to validate the scaling technology of the gas–gas combustor performance.

6.1. Experimental facility

A simplified schematic diagram of the testing system is shown in Fig. 9. The configuration of the multi-element chamber can be seen in Fig. 10. The chamber

was modular and could be easily configured to accommodate changes of injector, combustor and nozzle in geometrical configuration. The chamber was a heat-sink design. The size and the configuration of the injector and the combustor were designed to be the same as those of the prototype chamber studied numerically in the above section.

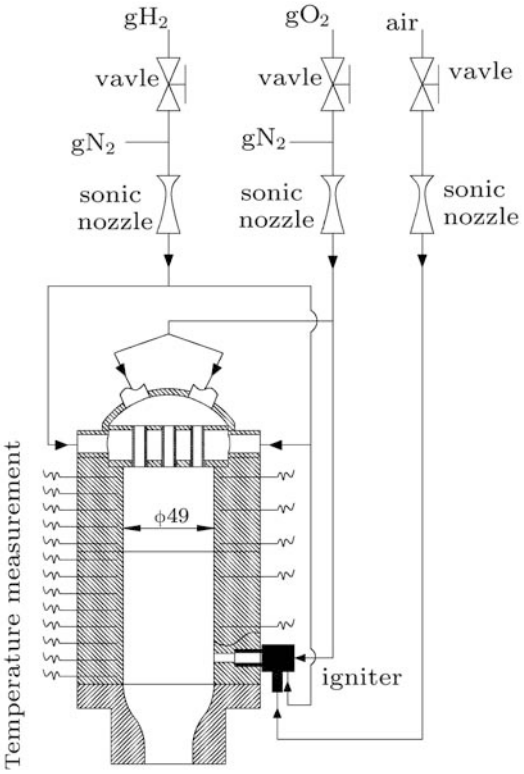


Fig. 9. Facility schematic diagram.

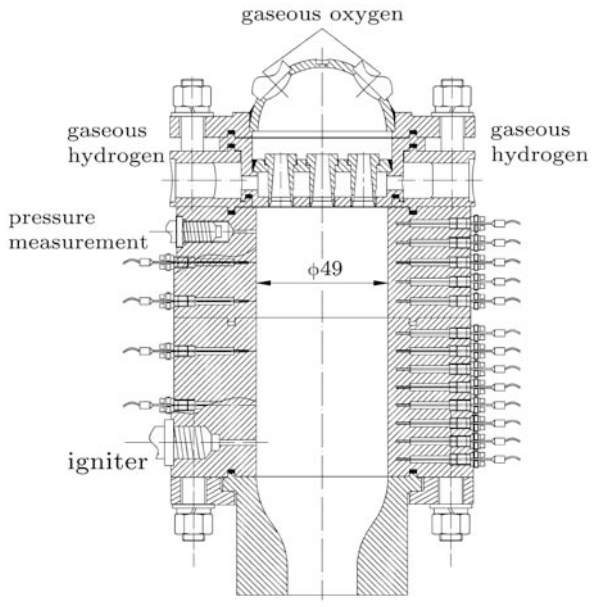


Fig. 10. Schematic diagram of multi-element chamber.

6.2. Results and discussion

By making full use of the capability of the experimental system, a hot-test with a maximum flowrate of 3.0 kg/s in this testing system was carried out. A total of nine hot-fire tests were conducted steadily. The operational conditions and the typical chamber pressure profiles are summarized in Table 5 and Fig. 11 respectively. The nominal values of mixture ratio (MR) are 6.0. The parameters in Table 5 imply that all the limiting conditions of scaling of the inner combustion flowfield are satisfied.

The testing combustion efficiencies η_{C*} for these cases were calculated with the following equations

$$\eta_{C^*} = \frac{C^*_{\rm Exp}}{C^*_{\rm Th}}, \tag{10}$$

$$C^*_{\rm Exp} = \frac{p_{\rm c} A_{\rm t}}{\dot{m}}, \tag{11}$$

$$C^*_{\rm Th} = \frac{\sqrt{RT_{\rm Th}}}{\Gamma}, \tag{12}$$

$$\Gamma = \sqrt{k}\left(\frac{2}{k+1}\right)^{(k+1)/2(k-1)}. \tag{13}$$

Here, $p_{\rm c}$ is the measurement hot-testing chamber pressure, $A_{\rm t}$ is the area of the chamber throat section, $\dot{m}$ is the measurement total mass flowrate of H_2 and O_2, k is the specific heat ratio, R is the universal gas constant of the product and $T_{\rm Th}$ is the theoretical combustion temperature at the given mixture ratio. The theoretical parameters of the combustion products were calculated from the Bolinkly method assuming perfect-mixing adiabatic combustion with the experimental chamber pressure and propellant inlet temperatures as input data. The hot-testing combustion efficiency of these cases were calculated and are shown in Table 6. The measurement errors for the chamber pressure and propellant mass flowrate are $\pm 0.2\%$ and $\pm 1.0\%$ respectively. From Table 6, the C^* efficiencies for all the cases ranging from 96.9% to 98.3% can be seen. They are much closer to each other, which validates the scaling technology obtained above: if the similarity conditions of inner flowfield are satisfied, the combustion performance will remain unchanged. The combustion performance of a high-pressure chamber totally can be substituted with that of a low-pressure chamber.

Table 5. Operational parameters of tests.

Chamber pressure /MPa	OX flowrate /g·s^{-1}	OX temperature /K	OX velocity /m·s^{-1}	Fuel flowrate /g·s^{-1}	Fuel temperature /K	Fuel velocity /m·s^{-1}	MR
1.51	1094	295	~ 60	186	305	~ 550	5.88
1.54	1111	295	~ 60	186	305	~ 550	5.97
2.05	1488	294	~ 60	243	306	~ 550	6.12
2.05	1486	294	~ 60	246	308	~ 550	6.04
2.61	1880	295	~ 60	314	308	~ 550	5.99
3.02	2170	296	~ 60	368	308	~ 550	5.90
3.06	2235	296	~ 60	362	308	~ 550	6.17
3.68	2614	294	~ 60	429	303	~ 550	6.09
3.68	2631	293	~ 60	432	302	~ 550	6.05

Table 6. C^* efficiencies of the hot-tests.

Chamber pressure/MPa	Experimental character velocity $C^*_{\rm Exp}$/m·s^{-1}	Theoretical character velocity $C^*_{\rm Th}$/m·s^{-1}	C^* efficiency η_{C^*}
1.51	2225	2293	97.0%
1.54	2239	2289	97.8%
2.05	2240	2285	98.0%
2.05	2240	2291	97.7%
2.61	2244	2304	97.4%
3.02	2245	2316	96.9%
3.06	2223	2289	97.1%
3.68	2269	2309	98.3%
3.68	2266	2311	98.1%

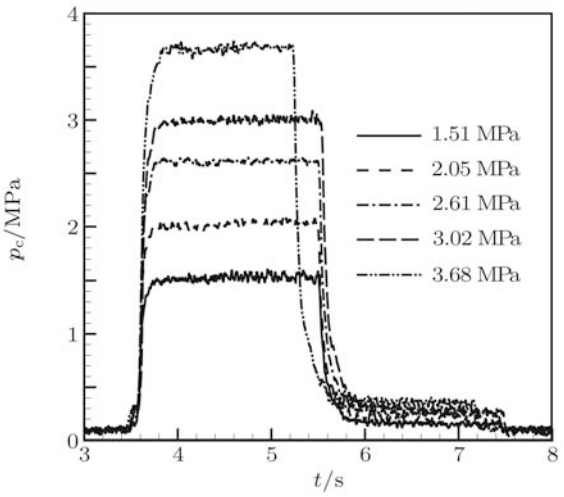


Fig. 11. Typical chamber pressure profiles for five typical hot-testing cases.

7. Conclusions

The scaling of gas–gas combustor performance was investigated systematically. The performance subelement analysis was conducted initially to obtain the key subelements. This needs further investigation individually when the inner main flowfield is similar. The theoretical scaling criterion of the gas–gas injector combustor performance could be obtained by conducting a detailed theoretical analysis of the key subelements, but it proves to be impractical. Further specific analyses of the key subelements themselves and their influences on the combustion performance in an LPRE combustor were carried out on the basis of the similarity of the inner combustion flowfield. Numerical and experimental studies of multi-element gas–gas injector chambers were conducted to verify the analysis result. Some conclusions are listed below.

(i) In an LPRE gas–gas injector combustor, when the main flowfield is similar, the scaling of combustion performance depends on the scaling of the inner wall friction and heat transfer.

(ii) The combustion performance of different-sized gas–gas injector combustors at different pressures will be similar as long as Re are kept unchanged when the main flowfield is similar. This conclusion is true for all the engines and combustion devices with gaseous fuels and oxidizers.

(iii) If the scaling criterion of inner combustion flowfield is satisfied, the friction stress distribution across the combustor inner wall will be qualitatively similar and any local friction stress correlates well with pressure and dimension as $\tau_{\rm w} \propto p^{0.8} d_{\rm t}^{-0.2}$. The wall-friction loss $\zeta_{\rm f}$ is proportional to $p_{\rm c}^{-0.2} d_{\rm t}^{-0.2}$ and the heat-transfer loss $\zeta_q \propto p_{\rm c}^{-0.1} d_{\rm t}^{-0.1}$. This result is valuable when the wall friction is the research object in a gas–gas combustion device.

(iv) When regenerative-cooling and the boundary layer correction design of the combustor physical profile are used, or the wall-friction and heat-transfer losses play minor roles in the combustion performance, the hot-testing combustion performance data from the low-pressure small-sized gas–gas combustion chamber can be exactly applied to a high-pressure full-scale chamber, which can greatly reduce the development cost and period or potential dangers.

Acknowledgments

The authors thank Beijing Space Propulsion Experiment Centre for the experimental facilities. The authors also thank W Zhang and S Li from Beijing West Zhonghang Technology Ltd for help in designing the thermocouples. Finally, the authors thank all the people who made contributions and helped with this paper.

References

[1] Dexter C E, Fisher M F, Hulka J R, Denisov K P, Shibanov A A and Agarkov A F 2004 *Liquid Rocket Thrust Chambers: Aspects of Modeling, Analysis and Design* ed. Yang V, Habiballah M, Hulka J and Popp M *Progress in Astronautics and Aeronautics* **200** p. 553

[2] Kenny R J, Moser M D, Hulka J R and Jones G 2006 *AIAA Paper* No. 4705

[3] Hulka J R 2008 *AIAA Paper* No. 5113

[4] Davis J A and Campbell R L 1997 *AIAA Paper* No. 3318

[5] Wim A, de Groot, Thomas J, McGuire and Steven J Schneider 1997 *AIAA Paper* No. 2847

[6] Calhoon D, Ito J and Kors D 1973 *NASA CR*-121234, Contract NAS3-13379

[7] Foust M J, Deshpande M, Pal S, Ni T, Merkle C L and Santoro R J 1996 *AIAA Paper* No. 0646

[8] Schley C A, Hagemann G and Tucker P K 1997 *AIAA Paper* No. 3302

[9] Tucker P K, Klemt M D and Smith T D 1997 *AIAA Paper* No. 3350

[10] Farhangi S, Yu T, Rojas L, Sprouse K and McKinnon J 1999 *AIAA Paper* No. 2757

[11] Archambault M R, Talley D and Peroomian O 2002 *AIAA Paper* No. 1088

[12] Smith T D, Klem M D and Breisacher K J 2002 *NASA/TM*-2002-211982

[13] Marshall W M, Pal S, Woodward R D and Santoro R J 2005 *AIAA Paper* No. 3572

[14] Lin J, West J S, Williamst R W, Tucker P K and Chenoweth J D 2005 *AIAA Paper* No. 4524

[15] Tucker P K, Menon S, Merkle C L, Oefelein J C and Yang V 2007 *AIAA Paper* No. 5572

[16] Tucker P K, Menon S, Merkle C L, Oefelein J C and Yang V 2008 *AIAA Paper* No. 5226

[17] Vaidyanathan R, Tucker P K, Papial N and Shyy W 2004 *J. Propul. Power* **20** 705

[18] Sozer E, Vaidyanathan A, Segal C and Shyy W 2009 *AIAA Paper* No. 0449

[19] Cai G B, Wang X W, Jin P and Gao Y S 2008 *AIAA Paper* No. 4562

[20] Wang X W, Cai G B and Gao Y S 2009 *AIAA Paper* No. 5042

[21] Wang X W, Gao Y S and Cai G B 2010 *J. Aerospace Power* **25** 691 (in Chinese)

[22] Wang X W, Gao Y S and Cai G B 2010 *J. Aerospace Power* **25** 1401 (in Chinese)

[23] Wang X W, Jin P, Zhang G Z and Cai G B 2008 *J. Propul. Technol.* **4** 407 (in Chinese)

[24] Wang X W, Jin P and Cai G B 2009 *J. Beijing University of Aeronautics and Astronautics* **35** 1095 (in Chinese)

[25] Wang X W, Jin P and Cai G B 2010 *Acta Aeronautica et Astronautica Sinica* **32** 1305 (in Chinese)

[26] Cai G B, Wang X W, Jin P and Gao Y S 2011 *J. Propul. Power* (accepted)

[27] Wang X W, Cai G B and Jin P 2010 *Chin. Phys.* B **19** 019401

[28] Wang X W, Cai G B and Gao Y 2011 *Chin. Phys.* B **20** 064701

[29] *JANNAF Rocket Engine Performance Prediction and Evaluation Manual* 1975 CPIA Publication p. 246

[30] Coats D E 2004 *Liquid Rocket Thrust Chambers: Aspects of Modeling, Analysis and Design* ed. Yang V, Habiballah M, Hulka J and Popp M *Progress in Astronautics and Aeronautics* **200** p. 601

[31] Huzel D K and Huang D H 1992 *Modern Engineering for Design of Liquid-Propellant Rocket Engines, Progress in Astronautics and Aeronautics* **147** AIAA, Washington, DC

[32] Gao Y W 2002 *Experimental Fluid Dynamics* (Xian: Northwestern Polytechnical University Press) (in Chinese)

[33] Pope S B 2000 *Turbulent Flows* (Cambridge: Cambridge University Press)

[34] Bian B M, He A Z, Li Z H, Yang L, Zhang P, Shen Z H and Ni X W 2005 *Acta Phys. Sin.* **54** 5534 (in Chinese)

[35] Liu G Q 1993 *Theory of Rocket Engines* (Beijing: Aerospace Press) (in Chinese)